Journal of Applied Fluid Mechanics, Vol. 9, No. 4, pp. 1655-1665, 2016.
Available online at www.jafmonline.net, ISSN 1735-3572, EISSN 1735-3645.
DOI: 10.18869/acadpub.jafm.68.235.24813

Oscillatory Magnetohydrodynamic Natural Convection of Liquid Metal between Vertical Coaxial Cylinders

F. Mebarek-Oudina[1†] and R. Bessaih[2]

[1]*Département des Sciences de la Matière, Faculté des Sciences, Université 20 août 1955 - Skikda,* B.P 26 Route El-Hadaiek, Skikda 21000, Algeria.
[2]*LEAP Laboratory, Department of Mechanical Engineering, Faculty of Sciences Technology, University of Frères Mentouri-Constantine, Route de Ain El. Bey, Constantine 25000, Algeria*

†*Corresponding Author Email: oudina2003@yahoo.fr*

(Received March 22, 2015; accepted September 1, 2015)

ABSTRACT

A numerical study of oscillatory magnetohydrodynamic (MHD) natural convection of liquid metal between vertical coaxial cylinders is carried out. The motivation of this study is to determine the value of the critical Rayleigh number, Ra_{cr} for two orientations of the magnetic field and different values of the Hartmann number ($Ha_r$and Ha_z) and aspect ratios A. The inner and outer cylinders are maintained at uniform temperatures, while the horizontal top and bottom walls are thermally insulated. The governing equations are numerically solved using a finite volume method. Comparisons with previous results were performed and found to be in excellent agreement. The numerical results for various governing parameters of the problem are discussed in terms of streamlines, isotherms and Nusselt number in the annuli. The time evolution of velocity, temperature, streamlines and Nusselt number with Ra_{cr}, Ha_r, Ha_z, and A is quite interesting. We can control the flow stability and heat transfer rate in varying the aspect ratio, intensity and direction of the magnetic field.

Keywords: MHD; Numerical modeling; Liquid metal; Natural convection; Hydrodynamic stability; Cylindrical annulus.

NOMENCLATURE

A	aspect ratio = H/D
B_0	intensity of magnetic field, Tesla
B_r	radial magnetic field, Tesla
B_z	axial magnetic field, Tesla
D	lengths
F	Lorentz force
g	gravitational acceleration
H	enclosure height
Ha	Hartmann number
J	electric current density
$\overline{Nu}$	average Nusselt number
P	dimensionless pressure
Pr	Prandtl number
Ra	Rayleigh number
r^*,z^*	radial and axial coordinates, respectively
r_i,r_0	inner and outer radii
t	dimensionless time
Δt	dimensionless time increment
T^*	temperature
T	dimensionless temperature
u^*	radial velocity
w^*	axial velocity
u,w	dimensionless radial and axial velocities, respectively
α	thermal diffusivity of the fluid
β	thermal expansion coefficient of the fluid
λ	radii ratio
ρ	density of the fluid
τ	time
σ	electric conductivity
υ	kinematic viscosity of the fluid
ψ	dimensionless stream function

Indices

cr	critical
C	cold
EM	electromagnetic
H	hot
r,z	radial and axial directions, respectively

1. INTRODUCTION

The combination of classical electromagnetism with fluid mechanics is the MHD. Magneto-hydrodynamics (MHD) domain is the interaction between the electric currents and magnetic field results in Lorentz body forces, in the presence of an external magnetic field, which, in turn, can be used to propel and manipulate fluids. A magnetic field imposed on electrically conducting fluid retards the motion perpendicular to this magnetic field (Mebarek-Oudina and Bessaih, 2014a).

The natural convection problem of a liquid metal in the presence of magnetic field has been the subject of many investigations. This is due to the important role it plays in industrial applications such as materials processing, crystal growth, nuclear engineering in connection with the cooling of reactors, safety aspect of gas-cooled reactors, solar energy collectors, and welding. Such configuration of space between concentric cylinders is also found in annular heat exchangers and various annuli configurations of turbo machinery.

The control of heat and mass transfers with the effect of a constant magnetic field on the liquid metal natural convection flows in various configurations was the subject of many studies (Mebarek-Oudina and Bessaih, 2014b; Kakarantzas *et al*., 2014; Kakarantzas *et al*., 2011; Sankar *et al*. 2011; Mebarek-Oudina and Bessaih, 2007a-b;Altintas and Ozkol, 2015).Sankar *et al*. (2006) numerically studied natural convection of an electrically conducting fluid in the presence of axial or radial magnetic field inside a vertical cylindrical annulus. They found that, the direction of magnetic field plays an important role in suppressing the convective flows. The heat transfer rate increases with radii ratio and decreases with the Hartmann numbers. Uda *et al*. (2000) experimentally investigated the MHD effect on heat transfer in liquid lithium annular flow with an emphasis on heat transfer enhancement and local turbulence. The heat transfer is observed to increase over a particular. This is explained as a result of local turbulence enhancement in the vicinity of the heating wall. Experimental studies on heat transfer in liquid Lithium flow is conducted to compare with earlier studies by Naoki *et al*. (2011).

Numerous studies were reported in the literature on natural convection between annulus spaces formed between circular cylinders. Anil Lal *et al*. (2013) presented a numerical prediction of natural convection flow in a vertical annulus closed at the top and opened at the bottom. The outer cylindrical surface of the annulus is cooled to a low temperature, and a hot fluid is maintained below the open-end temperature. Heat transfer through the annulus is subjected to sharp spatial variations due to the typical flow pattern at high values of Rayleigh number and is influenced by upstream conduction at low values of Rayleigh number. Correlations for average Nusselt number and volume rate of flow were obtained as functions of Rayleigh number and percentage gap ratio. Kuo and Leong (2013) obtained an analytical solution for a steady cylindrical magnetic Couette flow between two electrically insulated cylinders under the influence of a radial magnetic field. Their results showed that the primary flow characteristics could be effectively controlled through a good choice of the electric conductivities of the disk and cylinder walls. Gavara and Kanna (2012) studied numerically laminar natural convection between two coaxial vertical rectangular cylinders. At a given elevation, local Nusselt number on the inner cylinder faces increases towards cylinder edges. The effect of thermal condition of the walls of outer cylinder, inlet and outlet on the natural convection was analyzed.

The numerical investigation of the effect of radial or axial magnetic field on the double-diffusive convection in a cylindrical annular cavity by solving the complete Navier–Stokes equations for a wide range of physical parameters are carried out by Venkatachalappa *et al*. (2011). Heat and mass transfer, fluid flow results are presented in terms of streamlines, isotherms, average Nusselt and Sherwood numbers. For small buoyancy ratios, the magnetic field suppresses the double-diffusive convection, and it is effective when it is applied perpendicular to the main flow. Fattahi *et al*. (2010) simulated natural convection in eccentric annulus using the Lattice Boltzmann Model, in order to examine the effect of diagonal, vertical, and horizontal eccentricity at various locations on the convection. Their results showed that Nusselt number increases with lowering the inner cylinder independent of its radial position. Witkowski and Walker (2002) studied numerically the steady liquid metal flow between a pair of insulated cylinders subjected to a rotational motion and a uniform weak transverse magnetic field. The main flow pattern consisted of an axisymmetric part combined with a weak nonaxisymmetric part. Kumar and Kalam (1991) reported numerically generated heat transfer data for laminar natural convection in tall and short vertical annuli with isothermal vertical cylinders.

In the present work, a similar configuration for that use by Sankar *et al*. (2006) is considered where a liquid metal is placed inside two concentric vertical cylinders. Thus, heat transfer, MHD stability effects may be significantly different when in change of the aspect ratio. The effect of the magnetic field orientations, aspect ratio and thermal condition of the inner and outer cylinders on the stability of the flow is investigated. To our knowledge the MHD stability controlled with an aspect ratio of enclosure and the magnetic field directions in cylindrical annulus has never been the object of a preceding study, except thus studied by Mebarek-Oudina and Bessaih (2014a) in a cylindrical configuration and for the laminar case by Sankar *et al*. (2006).Our objective is to determine the critical Rayleigh numbers, Ra_{cr} associated with Hartmann numbers and different aspect ratios, showing the effect of radial (B_r) or axial (B_z) magnetic fields on the hydrodynamic and thermal stability.

The paper is organized as follows: The physical model and mathematical formulation are given in Section 2. Numerical solution, grid effect and

validation code are discussed in Section 3. The results and discussion are presented in Section 4. Finally, the conclusions are given.

2. PROBLEM FORMULATION

2.1 Geometry and Governing Equations

The schematic diagram of the flow configuration is shown in Fig. 1. System is a vertical cylindrical annulus formed by two concentric vertical cylinders of inner and outer radii r_i and r_o, respectively. The inner and outer walls of the annulus are maintained at isothermal, but different temperatures T_H^* and T_C^*, respectively, while the top and bottom of the annulus are assumed adiabatic. The annular cavity is filled with a low Prandtl number fluid (liquid metal, Pr=0.054), which is electrically conducting, and it is used as a coolant for thermodynamic systems in the nuclear reactors. The cylindrical coordinates (r,z) with corresponding velocity components (u^*,w^*) are as indicated in Fig. 1. The fluid is permeated by a uniform magnetic field B_0 along the $r^*$and z^* directions, parallel or perpendicular to gravity. The electrically conducting fluid interacts with an external uniform magnetic field of constant magnitude B_0. Thus, the Lorentz force depends only on the velocity component perpendicular to the magnetic field.

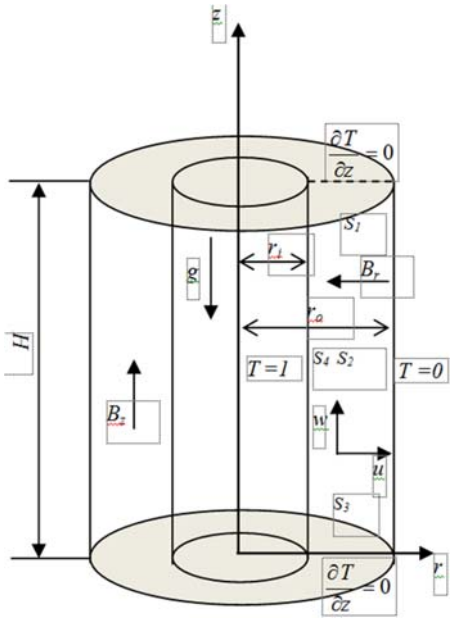

Fig. 1. Physical configuration and co-ordinate system, where S_1, S_2, S_3 and S_4 are the monitoring points of hydrodynamic and thermal instabilities detection.

Employing the Boussinesq approximation, the equations governing laminar, two-dimensional, axisymmetric flow of a Newtonian, electrically conducting fluid, after neglecting viscous and Ohmic dissipations, in cylindrical coordinates (r^*,z^*) are:

$$\frac{\partial(r^* u^*)}{\partial r^*}+\frac{\partial(r^* w^*)}{\partial z^*}=0 \tag{1}$$

$$\rho\left(\frac{\partial u^*}{\partial \tau}+u^*\frac{\partial u^*}{\partial r^*}+w^*\frac{\partial u^*}{\partial z^*}\right)=-\frac{\partial P^*}{\partial r^*}+f_{Lr}+\mu\left(\frac{1}{r^*}\frac{\partial}{\partial r^*}\left(r^*\frac{\partial u^*}{\partial r^*}\right)+\frac{\partial^2 u^*}{\partial z^{*2}}-\frac{u^*}{r^{*2}}\right) \tag{2}$$

$$\rho\left(\frac{\partial w^*}{\partial \tau}+u^*\frac{\partial w^*}{\partial r^*}+w^*\frac{\partial w^*}{\partial z^*}\right)=-\frac{\partial P^*}{\partial z^*}+\rho g\beta(T^*-T_C^*)+f_{Lz}+\mu\left(\frac{1}{r^*}\frac{\partial}{\partial r^*}\left(r^*\frac{\partial w^*}{\partial r^*}\right)+\frac{\partial^2 w^*}{\partial z^{*2}}\right) \tag{3}$$

where u^*, w^* are the components of the radial and axial velocities respectively, g is the gravity acceleration, β is the coefficient of volumetric expansion and ρ is the fluid density. f_{Lr}, f_{Lz} are the electromagnetic force components in (r^*,z^*) directions respectively. This EM force is given by the formula:

$$\overrightarrow{f_L}=\vec{j}\wedge\vec{B} \tag{4}$$

$$\frac{\partial T^*}{\partial \tau}+u^*\frac{\partial T^*}{\partial r^*}+w^*\frac{\partial T}{\partial z^*}=\alpha\left(\frac{1}{r^*}\frac{\partial}{\partial r}\left(r^*\frac{\partial T^*}{\partial r^*}\right)+\left(\frac{\partial^2 T^*}{\partial z^{*2}}\right)\right) \tag{5}$$

where, $\alpha=\kappa/\rho C_p$ is thermal diffusivity of the liquid, κ is the thermal conductivity and C_p its specific heat to constant pressure.

$D=r_0-r_i$, D^2/υ, υ/D, $\rho(\upsilon/D)^2$, $T_H^*-T_C^*$ as typical scales for lengths [m], velocities [m.s^{-1}], time [s], pressure [N. m^{-2}], and temperature [K], respectively.

The non-dimensional variables used in the present study are defined as follows:

$$t=\tau\Big/\frac{D^2}{\upsilon},\quad r=\frac{r^*-r_i}{D},\quad z=\frac{z^*}{D},\quad u=u^*/\left(\frac{\upsilon}{D}\right),\quad w=w^*/\left(\frac{\upsilon}{D}\right),\quad P=P^*/\rho\left(\frac{\upsilon}{D}\right)^2,\quad T=\frac{T^*-T_C^*}{T_H^*-T_C^*}$$

The dimensionless governing equations for the conservation of mass, momentum, and energy are written in dimensionless form, as follows:

$$\frac{\partial(ru)}{\partial r}+\frac{\partial(rw)}{\partial z}=0 \tag{6}$$

$$\frac{\partial u}{\partial t}+u\frac{\partial u}{\partial r}+w\frac{\partial u}{\partial z}=-\frac{\partial P}{\partial r}+\left(\frac{1}{r}\frac{\partial}{\partial r}\left(r\frac{\partial u}{\partial r}\right)+\frac{\partial^2 u}{\partial z^2}-\frac{u}{r^2}\right)+F_{EMr} \tag{7}$$

$$\frac{\partial w}{\partial t}+u\frac{\partial w}{\partial r}+w\frac{\partial w}{\partial z}=-\frac{\partial P}{\partial z}+\left(\frac{1}{r}\frac{\partial}{\partial r}\left(r\frac{\partial w}{\partial r}\right)+\frac{\partial^2 w}{\partial z^2}\right)+\frac{Ra}{\Pr}\cdot T+F_{EMz} \tag{8}$$

$$\frac{\partial T}{\partial t}+u\frac{\partial T}{\partial r}+w\frac{\partial T}{\partial z}=\frac{1}{\Pr}\left(\frac{1}{r}\frac{\partial}{\partial r}\left(r\frac{\partial T}{\partial r}\right)+\left(\frac{\partial^2 T}{\partial z^2}\right)\right) \tag{9}$$

where F_{EMr} and F_{EMz} represent the components of Lorentz force in r and z directions respectively, which are obtained using the equation: $F = J \times B$, where J and B are the electric current and magnetic field vectors, respectively [1]. The expressions of these components are:

- *Axial magnetic field :*

$$F_{EMr}=-Ha_r^2\cdot u \tag{10a}$$

$$F_{EMz}=0 \tag{10b}$$

- *Radial magnetic field:*

$$F_{EMr}=0 \tag{11a}$$

$$F_{EMz}=-Ha_z^2\cdot w \tag{11b}$$

The magneto convection problem in an annular cavity is, therefore, governed by the following non-dimensional parameters: $\Pr=\frac{\upsilon}{\alpha}$ is the Prandtl number, and $Ha=B_0\cdot D\sqrt{\sigma/\rho\upsilon}$ the Hartmann number, where υ is the kinematic viscosity and σ the electrical conductivity of the fluid. Ha_r and Ha_z are the Hartmann numbers due to radial and axial magnetic field, respectively. $Ra=\frac{g\beta(T_H-T_C)D^3}{\upsilon\alpha}$ is the Rayleigh number, $A=\frac{H}{D}$ the aspect ratio, and $\lambda=\frac{r_0}{r_i}$ the radii ratio.

The initial and boundary conditions in dimensionless form are:

at $t=0$, $u=w=T=0$ (12)

for $t\succ 0$,

at $r=1$: $u=w=0$, $T=1$ Hot inner wall (13a)

at $r=2$: $u=w=0$, $T=0$ Cold outer wall (13b)

at $z=0$: $u=w=0$, $\frac{\partial T}{\partial z}=0$ Bottom adiabatic wall (13c)

at $z=\frac{H}{D}$: $u=w=0$, $\frac{\partial T}{\partial z}=0$ Top adiabatic wall (13d)

The overall rate of heat transfer across the enclosure is expressed by the average Nusselt number at the hot cylindrical wall as

$$\overline{Nu}\big|_{r=1}=\int_1^2 Nu\cdot dz \tag{14}$$

where, $Nu=-\left.\frac{\partial T}{\partial r}\right|_{r=1}$ is the local Nusselt number

3. NUMERICAL SOLUTION

Numerical solutions of the governing equations (6)-(9), with the associated boundary conditions, are obtained using a finite-volume method. The components of the velocity (u and w) are stored at the staggered locations, and the scalar quantities (P and T) are stored in the center of these volumes (Mebarek-Oudina, 2014a).The numerical procedure called SIMPLER Patankar (1980)is used to handle the pressure-velocity coupling. The second-order accurate central difference scheme is used to discretize the convection and diffusion terms. The discretized difference equations are arranged in tridiagonal matrix that can be solved readily using the Thomas algorithm (TDMA). Convergence at a given time step is declared when the maximum relative change between two consecutive iteration levels fell below than 10^{-4}, for u, w and T. At steady, the calculations are effected with continuation until satisfaction of the convergence criteria, of determining the difference between the average Nusselt numbers on both walls (cold $\overline{Nu_C}$ and hot $\overline{Nu_H}$), and signal the stopping of calculations if the difference does not exceed a tolerance value δ :

$$\left|\overline{Nu_C}-\overline{Nu_H}\right|\le\delta \tag{15}$$

With:

$$\overline{Nu_H}=\sum\frac{[T(1,j)-T(2,j)]}{dr(1)}z_P(j)\Delta z(j) \tag{16}$$

$$\overline{Nu_C}=\sum\frac{[T(IL-1,j)-T(IL,j)]}{dr(IL-1)}z_P(j)\Delta z(j) \tag{17}$$

At the oscillatory regime (transient), the calculation is stopped after a number of long increment times enough to ensure that the oscillations obtained are physical in nature. Mass conservation is checked for each time increment Δt.

3.1 Grid Independence Study

Several non-uniform grids close to the cylinder walls, where large velocity and temperature gradients exist, thus require a larger number of nodes in order to resolve the specific characteristics of the MHD flow. They have been chosen according to geometric progressions, which permits a grid refinement near the walls. In order to examine the effect of the grid on the numerical solution and reduce numerical errors a number of grid sizes have been investigated for a grid independence study: 42×42 nodes, 72×72 nodes,

82×82 nodes and 82×164 nodes. By increasing the grid size from 72×72 nodes to 82×82 nodes or from 82×82 nodes to 164×164 nodes, a change of less than 2% in computed values was observed in Fig. 2. Therefore, in order to capture the Hartmann and side layers, the grid used has 82×82 nodes and was chosen after performing grid independence tests, since it is considered to have the best compromise between the computing time and the sufficient resolution in calculations. Calculations were carried out on a PC with CPU 3 GHz.

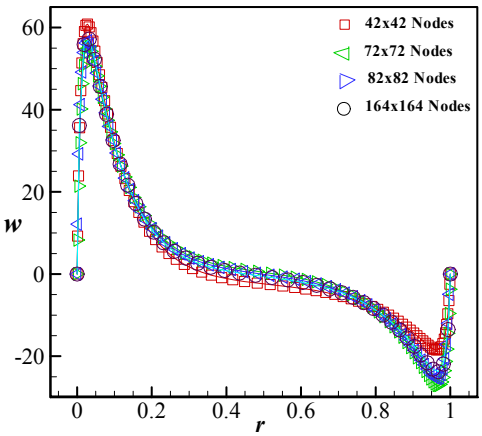

Fig. 2. Profiles of the dimensionless vertical velocity *w* with *r* for different grids, at *z*=0.5 for *Pr* =0.054, *Ra*=10^6, λ=2, *A*=1and *Ha*$_r$=100.

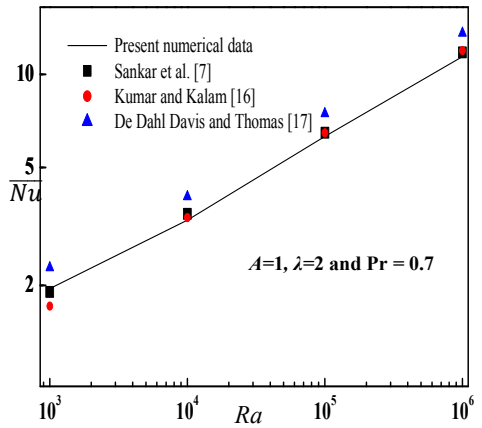

Fig. 3. Comparison of present results for heat transfer with data in the literature (*A*=1, *λ*=2 and *r* = 0.7).

3.2 Code Validation

The numerical technique of convection in a vertical annulus formed by two concentric cylinders is successfully investigated. The inner and outer cylinders are maintained at uniform temperatures, while the horizontal top and bottom walls are thermally insulated. However, in order to verify the accuracy of the current numerical results, simulations of the present model are tested and compared with different reference solutions available in the literature. First, the numerical results for different Rayleigh numbers are obtained. Figure 3 illustrates the variation of average Nusselt numbers with Rayleigh number. From this figure, the overall heat transfer rate increases with Ra.

To perform this validation, the comparison, shown in figure 3, reveals a good agreement between our results and that of Sankar *et al*. (2006), Kumar and Kalam (1991), and De Dahl Davis and Thomas (1969). In addition, we compare profiles of the temperature evolution with the results of Kumar and Kalam (1991) for *A*=1, λ=2 and *Ra* = 2 ×10^5 at z=0.5 (see Fig. 4). A very good agreement is obtained between the present numerical study and the numerical solution of Kumar and Kalam (1991).

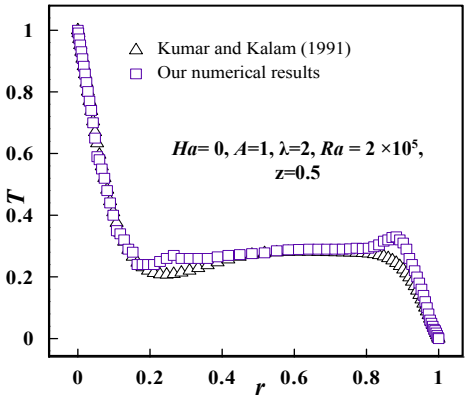

Fig. 4. Validation of computer code with the results of Kumar and Kalam (1991); Temperature profile for *Ha* = 0, *A*=1, λ=2 and *Ra* = 2 ×10^5 at *z*=0.5.

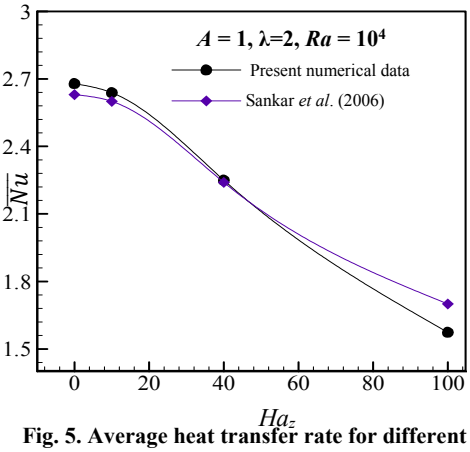

Fig. 5. Average heat transfer rate for different values of *Ha*$_z$, aspect ratio *A*=1, *Ra* = 10^4 and *Pr* = 0.054.

Without magnetic field, a good correspondence between our numerical results and literature data is found, what gives credibility to the present code.

The main effect of the magnetic field is to decrease the overall heat transfer rate between the hot and cold walls. The average local Nusselt number on the hot wall is calculated from the equation (14) and

presented in Fig. 5 for various magnetic field strengths. As *Ha* increases, the value of Nusselt numbers decreases. In the general cases, the effect of magnetic fields is to suppress the heat transfer and its effect is apparent in the Fig. 5 for axial magnetic field, unit aspect ratio and $Ra = 10^4$. This result is the same to the result found by Sankar *et al*. (2006).

4. RESULTS AND DISCUSSION

In the present work, we determine the physical instabilities within the flow from natural convection of a low Prandtl number fluid (Pr = 0.054), contained in a vertical cylindrical annulus with different aspect ratio A = 0.5, 1, 2. A constant magnetic field is projected on axial or radial direction of the flow. Then, the determination of physical instabilities is reduced to the determination of a Rayleigh number characterizing the subjacent flow, starting from which the flow becomes oscillatory. Numerical calculations are carried out by increasing the Rayleigh numbers to detect the physical instabilities.

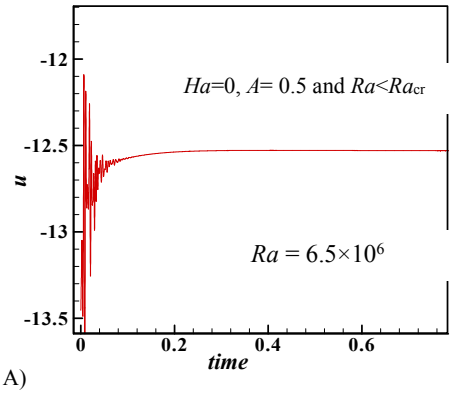

A)

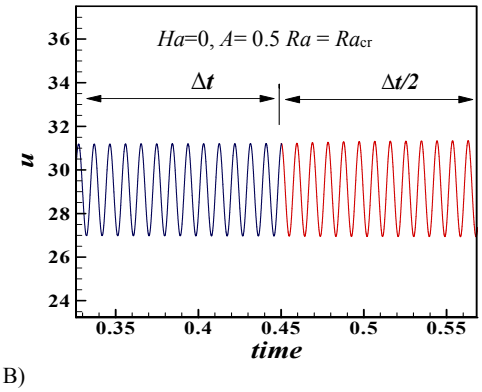

B)

Fig. 6. Comparison of the results between two time steps without magnetic field for the probe S_1, A=0.5 *a*) In steady state flow, $Ra<Ra_{cr}$. *b*) In oscillatory state flow, $Ra_{cr}= 6.65\times10^6$.

In order to eliminate a numerical solution, we use two dimensionless time step Δt and Δt/2. The physical solutions are defined for the same oscillations, or for the very low variations between the oscillations with Δt and Δt/2. Figure 6b presents examples of test Δt used in this study for Ha= 0. The results of both dimensional time steps Δt, Δt/2 are in quite good agreement. The results are considered as follows: First, we visualize of flow and thermal structures without a magnetic field. Next with a magnetic field, we determine the effect of axial and radial magnetic field. Finally, we study the effect of aspect ratio on stability flow in the presence of the magnetic field.

4.1 Results without Magnetic Field

In this section, Ha = 0 and the terms of the electromagnetic forces (the Lorentz forces F_{EMr} and F_{EMz}) are eliminated in Eqs. (8) and (9). At the onset of oscillatory flow, the calculation solution is found by determination of the critical Rayleigh number Ra_{cr}. For this, a small dimensionless time step ($\Delta t = 10^{-6}$) is necessary to make the transition as close as possible to the true case. In addition, to determine the amplitude and frequency when oscillations begin. The beginning of the oscillatory mode is possible with the increasing of the Rayleigh number starting from the steady solution, $Ra_{cr} = 6.65\times10^6$ (Figure 6b).

The steady state is limited by the value of the critical Rayleigh number ($Ra<Ra_{cr}$), the flow becomes oscillatory beyond this value (Figure 6a). At different dimensionless times, iso-contours of the dimensionless stream function and the isotherms are presented in figures 7, 8 and 12. The curves presented in Figure 7 (without magnetic field), Figure 8 (with axial magnetic field), and Figure 12 (with radial magnetic field) of the dimensionless radial velocity u, oscillate around the average values during a chosen interval of time. Its intensity is higher when the magnetic field is strongly present. When the flow becomes oscillatory and periodic in time, we determine the critical Rayleigh number Ra_{cr}.

Figure 7 presents the time evolution during one period of the dimensionless streamlines (defined as: $u = \partial\psi/\partial z$) for $Ra_{cr} = 6.65 \times 10^6$ and Ha = 0, and we indicate the various dimensionless times denoted by t_a, t_b, t_c . From this figure, the flow structure is represented by a cell located in the liquid part ($0< t < 0.6$). These cells generate a mass throughput of recirculation and an important convective transport located at the center of each of them. The variation of the dimensionless streamlines contours ψ, translates the periodic aspect of the flow. Here, the periodic regime is obtained and the physical quantities of oscillations are clearly deduced and presented.

Figures 8 and 12 show the time evolutions of the iso-contours of the dimensionless stream function ψ and isotherms. We can locate the maximum and minimum lines of stream function at the center of cells. The isotherms show clearly how the motion is driven. These figures show the streamlines hydrodynamic; iso-contours and isotherms. Over the dimensionless time (t_a, t_b, t_c), for a chosen period of oscillation. The lines of stream function are projected into the meridian plane (r^*,z^*). Then, noticing the oscillatory behavior of the various historical, we can see the establishment of an

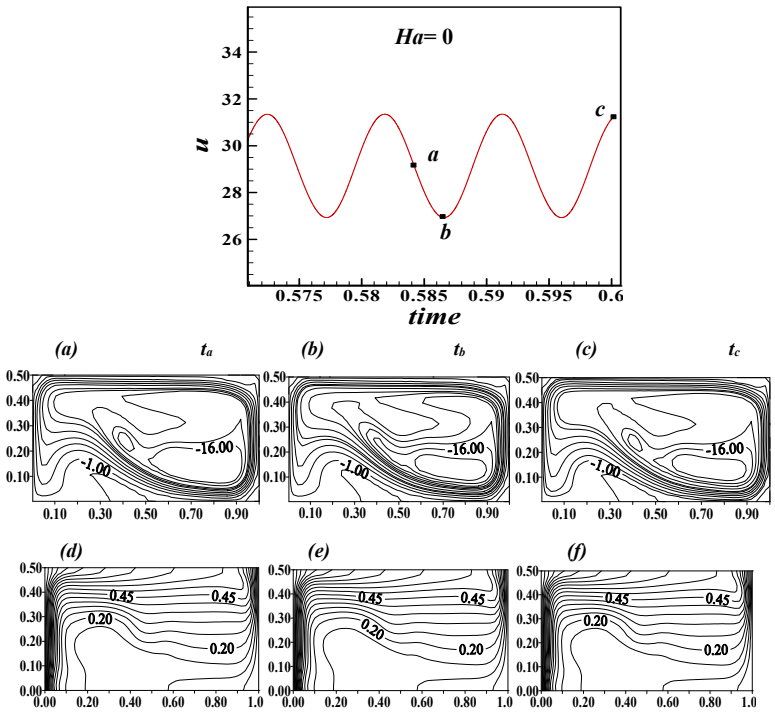

Fig. 7. Time evolution of the dimensionless radial velocity u for $Ha = 0$ (without magnetic field), $A = 0.5$ and $Ra_{cr} = 6.65\times10^6$ at the probe S_3. For various dimensionless times (t_a, t_b, t_c): (a), (b),(c) dimensionless streamlines ψ, (d),(e),(f) isotherms T.

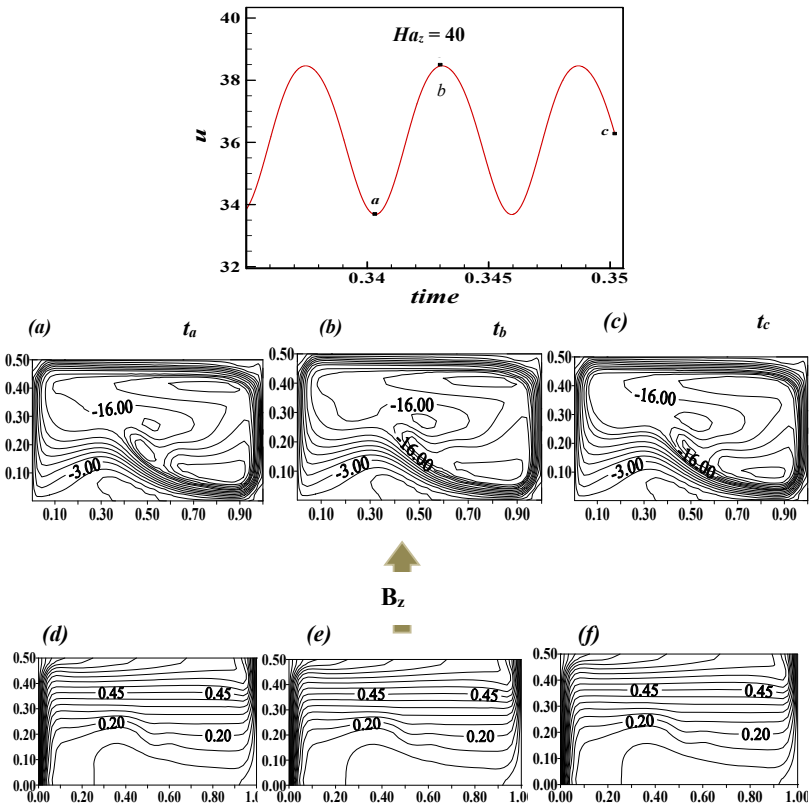

Fig. 8. Time evolution of the dimensionless radial velocity u for $Ha_z = 40$, $A = 0.5$ and $Ra_{cr} = 1.9\times10^7$ at the probe S_3. For various dimensionless times (t_a, t_b, t_c): (a), (b),(c) dimensionless streamlines ψ, (d),(e),(f) isotherms T.

unstable regime in the flow. This instability can be interpreted physically by the interaction of volume forces (Lorentz force) and buoyancy forces which gives rise to a multicellular flow. The stability is provided by the equilibrium between viscous and electromagnetic forces.

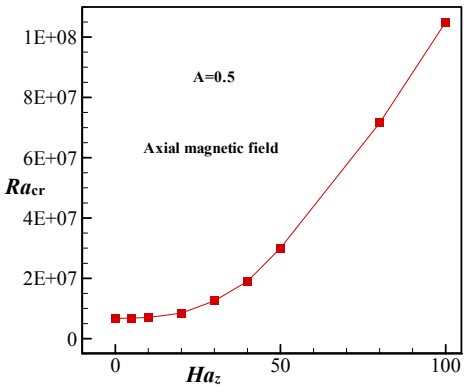

Fig. 9. Stability diagram Ra_{cr}–Ha_z for A=0.5.

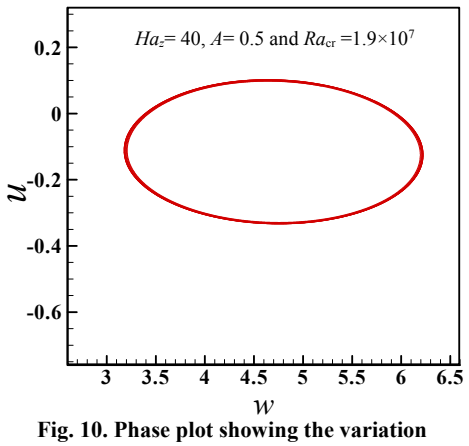

Fig. 10. Phase plot showing the variation between u and w for Ha_z= 40, A = 0.5 and Ra_{cr} =1.9×10^7.

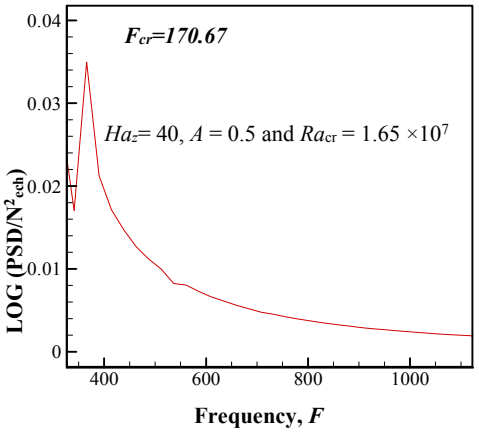

Fig. 11. Power spectrum of the dimensionless radial velocity u for Ha_z = 40 and A = 0.5. F_{cr} = 170.67 represents the dimensionless critical frequency.

The deformation of the isotherms (Figs. 7, 8 and 12) proves the existence and dominance of the convective to the diffusive regimes. We could consider from these figures that the application of a magnetic field makes the system more significant. This is due to increasing values of Rayleigh, which promotes the convective relative to diffusive fluxes.

4.2 Results with Magnetic Field

4.2.1 Effect of Axial Magnetic Field

The stratification of the temperature field in the interior begins to diminish. Figure 8 shows the isotherms and streamlines for Ha_z = 40. From this figure, we see that, the isotherms shown are parallel to the horizontal walls, begin from the top wall and will finish at the bottom wall, indicating that most of the heat transfer is by heat conduction. The fluctuation of unsteady dimensionless radial and axial components of velocity at a probe S_1 is presented in the form of a phase plot in Figure 10. A repeating loop obtained in the phase plot indicates that the unsteady flow is periodic.

4.2.2 Effect of Radial Magnetic Field

The hydrodynamic flow and thermal fields inside the annular enclosure are exemplified by the streamlines and isotherms in Fig. 7 without magnetic field, Fig. 8 with Ha_z= 40, and with Ha_r= 40 in Fig. 12. These figures show clearly the effect of magnetic field directions on the flow pattern and temperature distribution.

Plotted of the dimensionless velocity components in the phase planes (using the dynamical systems terminology), are presented in Figures 10 and 14. These diagrams called phase portraits are closed loops with dominant harmonics, which means that the quasi-periodic flow regime is reached. The phase portraits are used to inspect an intuitive and reliable of the movement regime, the addition of this utility, we used the phase portraits during calculations to ensure that the amplitudes are uniform or, the temporal evolutions have sinusoidal character. Exactly, you can see this periodic character behind the cycles limit.

In order to verify the effect of the magnetic field direction, we presented the tori in the plan (u,w) of the probe S1 for Ha_z = 40 and Ha_r = 40. The different parameters vary in a cyclical manner, thereby justifying the oscillatory character seen on the curves of time evolution.

In order to obtain the frequency of oscillation for the critical value, the discrete Fourier transform was used of a certain number N, which has to be a power of 2. This transform is multiplied by its combined complex and is divided by 2 to obtain the energy E, according to the frequencies of oscillations F, defined by F = M/ (NΔt), where Δt is the dimensionless time step and M = 0, 1, N=2. The values of E (F) represent several scales of sizes; in this case we use the decimal logarithm. Note that in this work, the peak of the energy spectrum, which corresponds to the major frequency F_{cr} for N = 2^{16} and Δt = 2.5×10^{-6} (Figs. 11 and 15) shows the

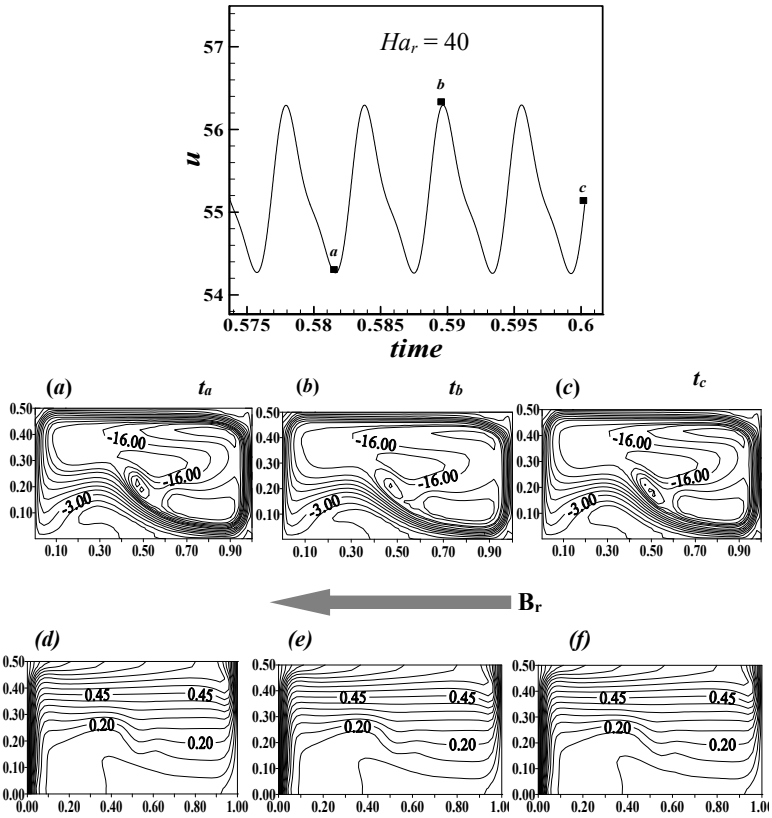

Fig. 12. Time evolution of the dimensionless radial velocity u for $Ha_r = 40$, $A = 0.5$ and $Ra_{cr} = 1.5 \times 10^7$ at the probe S_3. For various dimensionless times (t_a, t_b, t_c): (a), (b),(c) dimensionless streamlines ψ, (d),(e),(f) isotherms T.

prevalent frequencies of oscillations for some cases of the oscillatory flow (Mebarek-Oudina and Bessaih, 2014a).

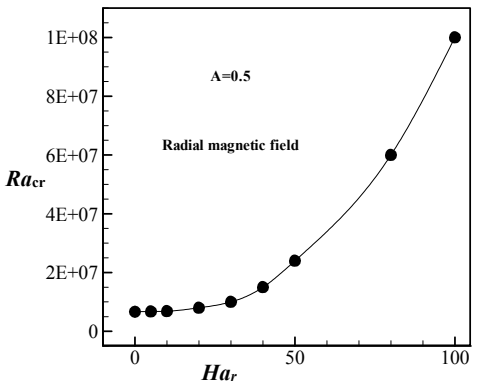

Fig. 13. Stability diagram Ra_{cr}–$Ha_r$for A=0.5.

4.2.3 Effect of Aspect Ratio

A numerical results are presented in Figs. 16-17, as the aspect ratio is increased from A = 0.5 to 2. Figures 16-17 show the effect of various aspect ratios (A=0.5, 1, and 2) on the values of the critical Rayleigh numbers, Ra_{cr}. We observe that the increase of A causes the decrease of the critical Rayleigh number. Since the direction of primary flow is along the two horizontal walls, the axial magnetic field is more effective for the shallow cavities. The strong magnetic field is required to suppress the flow for a higher Rayleigh number (Figs. 16-17).

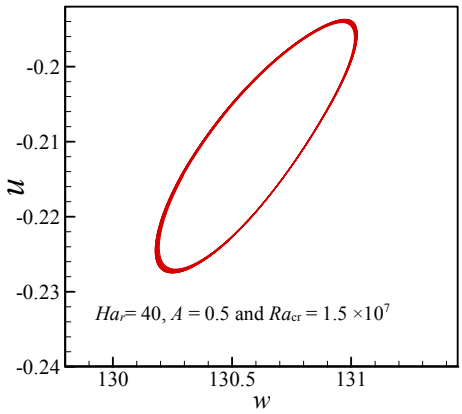

Fig. 14. Phase plot showing the variation between u and w for Ha_r= 40, A = 0.5 and Ra_{cr} =1.5×10^7.

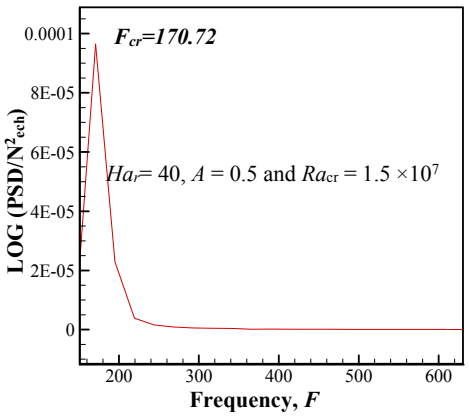

Fig. 15. Power spectrum of the dimensionless radial velocity u for Ha_r= 40 and A = 0.5. F_{cr} = 170.72 represents the dimensionless critical frequency.

At the onset of instability, for a given value of Hartmann number it can be seen that Ra_{cr} is a decreasing function of Ha_r and Ha_z. As expected, for a given value of aspect ratio, Ra_{cr} is an increasing function of Ha_z (Fig. 9) and Ha_r (Fig. 13) due to the fact of reducing the convection by the magnetic field. The effect of both radial and axial magnetic fields is approximately the same for aspect ratio equal to 1 (Fig. 16). However, generally, irrespective of direction, his role is to suppress the heat transfer.

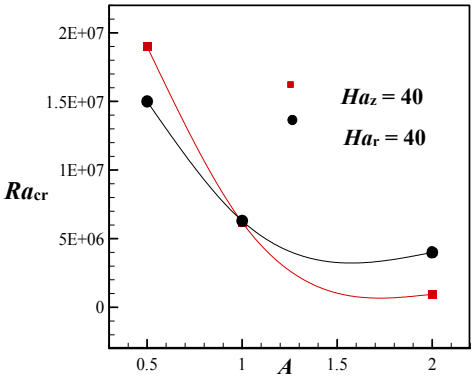

Fig. 16. Stability diagram Ra_{cr}–A for Ha_r=40 and Ha_z= 40.

5. CONCLUSION

A numerical study of natural convection in a vertical annulus formed by two concentric vertical cylinders is carried out. The inner and outer walls of the annulus are maintained at isothermal different temperatures, while the top and bottom of the annulus are adiabatic. The constant magnetic field has a harmful effect on the natural convection stability flows of the liquid metals, with a low Prandtl number (semiconductor, coolant). Whereas, the axial magnetic field is effective in suppressing heat transfer in shallow cavities and radial magnetic field for tall cavities.

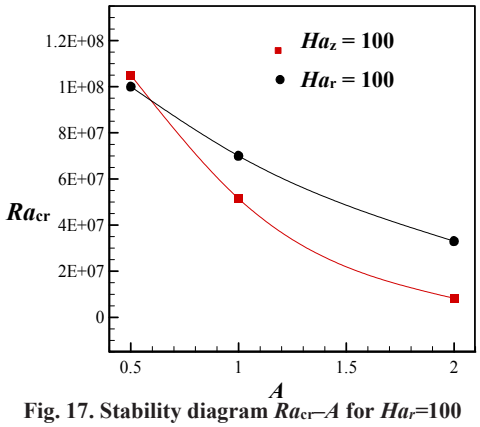

Fig. 17. Stability diagram Ra_{cr}–A for Ha_r=100 and Ha_z=100.

From the investigation, some conclusions can be summarized as follows:

- The increasing of the criticize Ra numbers with the values of the Hartmann number. For different aspect ratios and the magnetic field directions used in this study, the magnetic field has a stabilizing effect for this kind of flow.
- The decrease of critical Rayleigh numbers, with the increase of aspect ratio values. The increasing of the aspect ratio has a destabilizing effect for MHD flows in an annular space between two coaxial vertical cylinders, the inside is hot and the outside is cold.
- The importance of the magnetic field direction to eliminate the convective flows.
- When the magnetic field is perpendicular to the direction of the primary flow (radial field A=1, 2) and (axial field for A=0.5), it has a more stabilizing effect of the flow.
- The numerical results found in this numerical study have a good agreement with those found in the literature, with and without magnetic field.
- The effect of the magnetic field is to decrease the rate of convective heat transfer. The average Nusselt number decreases with an increase in Hartmann number.

ACKNOWLEDGEMENTS

The authors gratefully acknowledge the financial support of this work through the Algerian Ministry of Higher Education and Scientific Research.

REFERENCES

Altinas, A. and I. Ozkol (2015). Magnetohydrodynamic Flow of Liquid-Metal in circular Pipes of Externally Heated and Non-Heated cases. *Journal of Applied Fluid Mechanics* 8(3), 507-514.

Anil Lal, S. and V. A. Kumar (2013). Numerical Prediction of Natural Convection in a Vertical Annulus Closed at Top and Opened at Bottom.

Heat Transfer Engineering 34(1), 70-83.

De Vahl Davis, G. and R. W. Thomas (1969). Natural Convection between Vertical Cylinders. In High speed computing in fluid dynamics. *Phys. Fluids* (Supplement-II), 198–207.

Fattahi, E., M. Farhadi and K. Sedighi (2010). Lattice Boltzmann Simulation of Natural Convection Heat Transfer in Eccentric Annulus. *International Journal of Thermal Sciences* 49(12), 2353–2362.

Gavara, M. and P. R. Kanna (2012). Study of Conjugate Natural Convection between Vertical Coaxial Rectangular Cylinders. *International Communications in Heat and Mass Transfer* 39, 904–912.

Kakarantzas, S. C., I. E. Sarris and N. S. Vlachos (2011). Natural Convection of Liquid Metal in a Vertical Annulus with Lateral and Volumetric Heating in the Presence of a Horizontal Magnetic Field. *Int. J. Heat Mass Transfer* 54, 3347–3356.

Kakarantzas, S. C., I. E. Sarris and N. S. Vlachos (2014). Magnetohydrodynamic Natural Convection of Liquid Metal between Coaxial Isothermal Cylinders Due to Internal Heating. *Numerical Heat Transfer, Part A* 65, 401–418.

Kumar, R. and M. A. Kalam (1991). Laminar Thermal Convection between Vertical Coaxial Isothermal Cylinders. *Int. J. Heat Mass Transfer* 34(2), 513–524.

Kuo, J. S. and J. C. Leong (2013). Analysis of a Conducting Fluid in a Thin Annulus with Rotating Insulated Walls Under Radial Magnetic Effect, *Applied Mathematical Modelling* 37, 3021–3035.

Mebarek-Oudina, F. and R. Bessaïh (2007b). Stabilité Magnétohydrodynamique des Écoulements de Convection Naturelle dans une Configuration Cylindrique de type Czochralski. *Société Française de Thermique* 1, 451-457.

Mebarek-Oudina, F. and R. Bessaïh (2014a). Numerical Modeling of MHD Stability in a Cylindrical Configuration. *Journal of the Franklin Institute* 351(2), 667–681.

Mebarek-Oudina, F. and R. Bessaïh (2014b). Effect of the Geometry on the MHD Stability of Natural Convection Flows. *Institute of Thermomechanics AS CR, v. v. i.*, Prague. (75), 159-161.

Mebarek-Oudina, F., and R. Bessaïh (2007a). Magnetohydrodynamic Stability of Natural Convection Flows in Czochralski Crystal Growth. *World Journal of Engineering* 4(4), 15–22.

Naoki, U., M. Akira, I. Shoji, Y. Nabuo, H. Hiroshe and M. Keiji (2011). Forced Convection Heat Transfer and Temperature Fluctuations of Lithium under Traverse Magnetic Field. *J. Nuclear Science Technology* 38(11), 936-945.

Patankar, S. V. (1980). Numerical Heat Transfer and Fluid Flow, Hemisphere, Washington, DC.

Sankar, M., M. Venkatachalappa and I. S. Shivakumara (2006). Effect of Magnetic Field on Natural Convection in a Vertical Cylindrical Annulus. *International Journal of Engineering Science* 44, 1556–1570.

Sankar, M., M. Venkatachalappa and Y. Do (2011). Effect of Magnetic Field on the Buoyancy and Thermocapillary Driven Convection of an Electrically Conducting Fluid in Annular Enclosure. *International Journal of Heat and Fluid Flow* 32, 402–412.

Uda, N., M. Hayase, T. Chikaoka, S. Inoue, H. Horiike and K. Miyazaki (2000). Natural Convective Heat Transfer of Lithium under Magnetic Field. *Fusion Eng. Design* 51-52(3), 893-898.

Venkatachalappa, M., Y. Do and M. Sankar (2011). Effect of Magnetic Field on the Heat and Mass Transfer in a Vertical Annulus. *International Journal of Engineering Science* 49, 262–278.

Witkowski, L. M. and J. S. Walker (2002). Numerical Solutions for the Liquid-Metal Flow in a Rotating Cylinder with a Weak Transverse Magnetic Field. *Fluid Dynamics Research* 30, 127–137.